Simple Semianalytical Septum Design for Improved Matching in Open TEM Cells

Giacomo Giannetti, *Graduate Student Member, IEEE*, Christian Spindelberger, *Student Member, IEEE*, and Holger Arthaber, *Senior Member, IEEE*

***Abstract*—Open transverse electromagnetic (TEM) cells are used for many applications. Usually, such cells are built of metal sheets with linear profiles. Due to these simple geometries, impedance matching is limited. To improve the matching, a simple semianalytical method for an advanced septum profile is developed. Dominant TEM-mode propagation and an expression for the characteristic impedance of a stripline are considered. The characteristic impedances of the feed and the central stripline are equal to a given, desired value. To minimize reflections, the characteristic impedance of the TEM mode is enforced to be constant over the entire structure, especially along the tapered sections. In this way, the proposed method returns the septum width as a function of the longitudinal coordinate along the cell, such that each cross section has a characteristic impedance equal to the given, desired value. A septum designed according to the proposed method is manufactured and installed in a TEM cell prototype. The 30 MHz–1 GHz frequency range is considered to cover *CISPR* bands C and D. Both measurements and full-wave simulations indicate an improvement in the return loss of 4.6 dB from 10.6 to 15.2 dB with respect to the previously installed linearly tapered septum. Code supporting the findings available at: https://codeocean.com/capsule/4880490/tree.**

***Index Terms*—Design methodology, electromagnetic compatibility and interference (EMC/EMI), impedance matching, mathematical models, stripline, transverse electromagnetic (TEM) cells.**

I. Introduction

TRANSVERSE electromagnetic (TEM) cells are devices used to generate highly uniform field patterns. As TEM cells are easy to build and low cost, they are used in a wide variety of applications. For instance, they are successfully used for dielectric characterization [1], [2] in [3]; for biological cell exposure in [4]; and for electromagnetic-compatibility/electromagnetic-interference (EMC/EMI) precompliance tests in [5] and [6].

The key parameters describing the performance of TEM cells are impedance matching, bandwidth, field homogeneity, and usable test volume. These parameters are strongly coupled. Indeed, the bandwidth and the field homogeneity decrease for a larger test volume due to the excitation of higher-order modes [7], and a better impedance matching implies a better field homogeneity [8]. The impedance matching is quantified in terms of return loss (RL). TEM cells' RL should be at least 10 dB [9]. However, there is a great interest in further improving matching due to certain EMC standard requirements. For instance, [10] indicates that an RL of at least 14 dB is desirable. Besides, better impedance matching leads to less absolute measurement uncertainties due to load mismatches [11].

In TEM cells, a very critical part of the degradation of RL is the tapering [10], [12], which connects the feed with the central stripline. Several works operate on the tapering to improve the RL. In [10], the original linear straight tapering from [13] is studied extensively with a special focus on its start and end points. On the other hand, in [12], different arguments based on the characteristic impedance along the septum are analyzed to improve matching by means of both multistep and piecewise linear tapering. Both [10] and [12] rely on optimizations performed over computationally expensive full-wave simulations and are time consuming therefore.

Regarding the rigorous semianalytical modeling of the TEM cell, mode matching [14] is applied in [15] to analyze closed TEM cells. However, open TEM cells, as those considered in our work, have openings that partially radiate. To consider this, a more sophisticated mode-matching analysis, taking a continuous mode spectrum into account, would be required.

In our work, we focus on reflection reduction in open TEM cells by continuously modifying the septum geometry. This task is solved by means of a simple yet accurate

Take-Home Messages:

- Interest in improving TEM cell's impedance matching to improve field homogeneity and to reduce absolute measurement uncertainties
- Development of a new and simple semi-analytical design method for the septum's profile design
- Saving computational resources by avoiding expensive full-wave simulations and optimizations
- Validation of the method by improving an already existing TEM cell design
- Simulation and measurement results indicate a return loss increase of 4.6 dB from 10.6 dB to 15.2 dB with respect to the linearly tapered septum in the 30MHz – 1 GHz frequency range (*CISPR* bands C and D)

Manuscript received 11 September 2023; revised 16 October 2023; accepted 13 November 2023. Date of publication 15 November 2023; date of current version 8 March 2024. This work was supported by the Interreg EFRE Foundation through Project AMOR under Grant ATCZ-203. *(Corresponding author: Giacomo Giannetti.)*

Giacomo Giannetti is with the Department of Information Engineering, University of Florence, 50121 Florence, Italy (e-mail: giacomo.giannetti@unifi.it).

Christian Spindelberger and Holger Arthaber are with the Department of Electrodynamics, Microwave and Circuit Engineering, Technical University of Vienna, 1040 Vienna, Austria.

Digital Object Identifier 10.1109/LEMCPA.2023.3333003

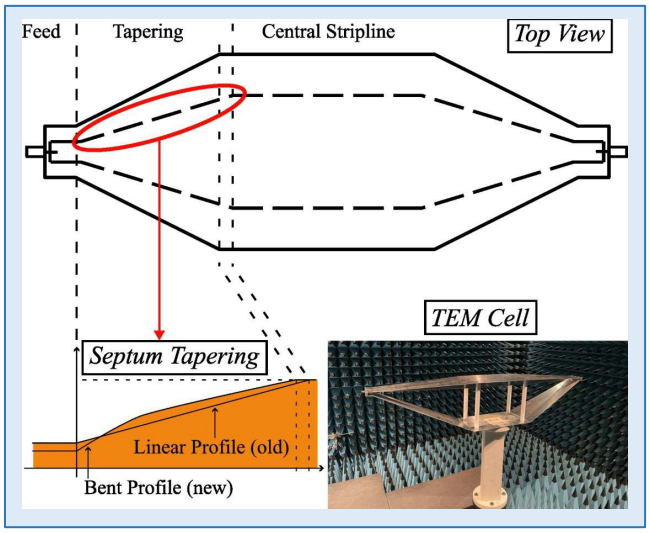

Fig. 1. Visual summary.

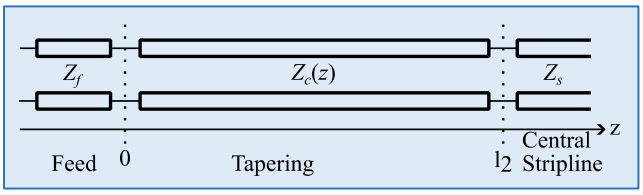

Fig. 2. Transmission-line schematic of the problem.

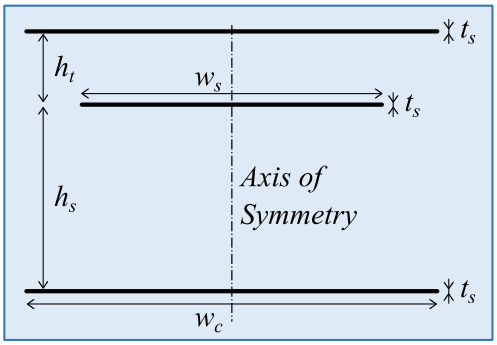

Fig. 3. Stripline cross section.

semianalytical method. We tackle the inherent difficulties of radiative and higher-order modes by assuming that the TEM-mode propagation is dominant over the higher-order modes. Particularly, based on an analytical expression for the characteristic impedance of the TEM cell's cross section, a near-optimum profile for impedance matching within the tapering section is derived. The method requires no optimization and, therefore, the number of full-wave simulations is reduced. The proposed method is first derived for a generic case in Section II and second applied to the specific open TEM cell from [16] in Section III. Eventually, conclusions are drawn in Section IV, and the present work is summarized graphically in Fig. 1.

II. Septum Design

TEM cells are composed of three parts: 1) the feed; 2) the tapering; and 3) the central stripline, as depicted in Fig. 1. All parts are striplines. However, the feed and the central stripline have constant transverse dimensions along the direction of propagation while the tapering has varying transverse dimensions to connect the narrow feed to the wide central stripline. In particular, the outer conductors are parallel to the septum for the feed and central stripline parts while this does not apply for the tapering sections. The three parts are connected such that the septum remains flat along the entire TEM cell, and the outer conductors are bent to connect the feeds and the central stripline. For further details about the design of the TEM cell, please refer to [16].

Exploiting transmission-line theory and if the TEM mode is dominant over the higher-order modes, the problem, neglecting the higher-order modes, is visualized from an electrical perspective in Fig. 2. The feed and the central stripline have a z-independent characteristic impedance equal to Z_f and Z_s, respectively. On the other hand, the tapering has a z-dependent characteristic impedance $Z_c(z)$ and ranges from $z = 0$ to $z = l_2$. The problem of joining two different waveguides with minimum reflections is well known [17]. Particularly, if the characteristic impedances of the two waveguides are equal, that is, $Z_f = Z_s$, then the optimum matching section is the one with a constant characteristic impedance equal to those of the two waveguides. If $Z_f = Z_s = Z_d$, where Z_d is a desired value, then the characteristic impedance along the tapering that minimizes the reflections is equal to $Z_c = Z_d$ for each longitudinal coordinate z between 0 and l_2.

A generic stripline cross section is depicted in Fig. 3. The outer conductors are grounded. Parameters describing the stripline cross section are the distance between the upper conductor and septum h_t, the septum height h_s, the width of the outer conductors w_c, the width of the septum w_s, and the thickness of the septum and outer conductors t_s. The background material has $\varepsilon_r = 1$ and $\mu_r = 1$. Generally speaking, the characteristic impedance for the TEM mode of the stripline depends on all the geometrical parameters of the stripline cross section and writes

$$Zc = Zc(h_t, h_s, w_c, w_s, t_s). \tag{1}$$

In the tapering, the quantities h_t, h_s, w_c, and w_s depend on the longitudinal coordinate z, while the thickness t_s is constant.

There are three ways to achieve a constant characteristic impedance equal to Z_d along the tapering of the cell. They are 1) bend one or both outer conductors and keep a linear straight septum profile; 2) keep linear straight outer conductors and modify the septum profile; and 3) modify the other conductors' width. In case 1), we would vary h_t or h_s, in case 2), w_s, and in case 3), w_c. All solutions are equivalent from an electrical point of view. However, approach 2) is the easiest to implement in practice and, hence, pursued in our work.

A pictorial representation of the problem is drawn in Fig. 4. In the upper graph of Fig. 4, the lateral view of the TEM cell is shown. The longitudinal coordinate $z = 0$ mm is aligned with the end of the feed and the beginning of the tapering. The end of the bends of the outer conductors is at $z = l_1$

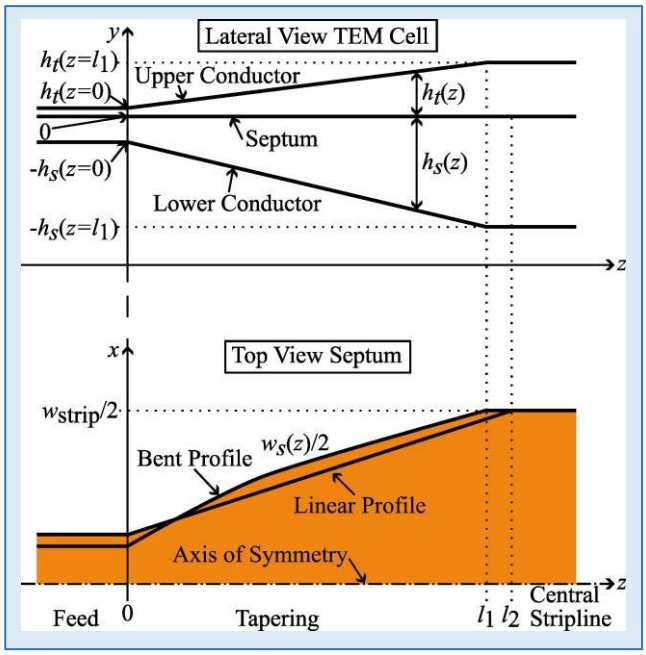

Fig. 4. Visualization of the design problem for the advanced septum profile.

while the tapering of the septum is in 0 mm $\leq z \leq l_2 \neq l_1$. This is the same as in the original approach by Crawford [13]. However, in the proposed approach, the tapering ends and the septum reaches the maximum width at $z = l_1$, since constant distances between the outer conductors and the septum for $z \geq l_1$ imply a constant width for the septum itself in the range $l_1 \leq z \leq l_2$. The lower graph in Fig. 4 depicts the top view of the septum.

The boundary conditions of the problem are as follows: h_t and h_s at $z = 0$ mm and at $z = l_1$ are given; the stripline width of the central stripline $w_s(z = l_1)$ is also given and is such that it realizes the desired characteristic impedance in the central stripline; the end coordinate of the tapering l_1 is provided. Expressions for the quantities $h_t(z)$, $h_s(z)$, and $w_c(z)$ are also given. Eventually, enforcing the condition $Z_c(z) = Z_d$ along the tapering, an explicit equation with a unique solution defining an implicit function for $w_s(z)$ is found. Particularly, for a given longitudinal coordinate $\bar{z}$, (1) becomes

$$Zc(h_t(\bar{z}),\ h_s(\bar{z}), w_c(\bar{z}), w_s(\bar{z}),\ t_s) = Z_d \tag{2}$$

and can be solved for $w_s(\bar{z})$. Assuming that the tapering is gradual and that it is long enough for the stabilization of the field mode, the solution to (2) for all z between 0 mm and l_1 returns a near-optimal septum profile for RL maximization.

III. Results

The proposed method is now applied to the TEM cell described in [16]. For this case, we have $l_1 = 621.9$ mm, $t_s = 3$ mm, $h_t(z = 0\text{ mm}) = 7$ mm, $h_t(z = l_1) = 41.4$ mm, $h_s(z = 0\text{ mm}) = 10$ mm, and $h_s(z = l_1) = 300$ mm. For the new septum, it is $l_2 = l_1$ while it is $l_2 = 641.9$ mm for the one presented in [16]. The width of the septum in the central stripline, realizing the desired characteristic impedance, is $w_s(z = l_1) = 195$ mm. The y-distance between the upper conductor and septum $h_t(z)$ and the one between the lower conductor and septum $h_s(z)$ (see Fig. 4) vary linearly in the interval 0 mm $\leq z \leq l_1$ according to

$$h_t(z) = h_t(z = 0\text{ mm}) + \frac{z}{l_1}(h_t(z = l_1) - h_t(Z = 0\text{ mm})) \tag{3a}$$

$$h_s(z) = h_s(z = 0\text{ mm}) + \frac{z}{l_1}(h_s(z = l_1) - h_s(Z = 0\text{ mm})). \tag{3b}$$

Among all the formulas for the computation of the characteristic impedance (1), for example, [18] and [19], the one in [20] is considered in the following since it represents a good compromise between accuracy and implementation complexity. The characteristic impedance for the TEM mode of the stripline writes (from [20, eq. (2)])

$$Zc = Z_0\left(\frac{(w/b)_{\text{eff}}}{\gamma} + \frac{(w/b)_{\text{eff}}}{\beta - \gamma} + \frac{2C_f'}{\varepsilon_0}\right)^{-1} \tag{4}$$

where ε_0 is the vacuum permittivity, and $(w/b)_{\text{eff}}$, γ, β, and C_f' are quantities depending on the geometrical parameters h_s, h_t, w_s, and t as defined in [20]. In (4), an infinite width for the outer conductors of the stripline ($w_c = \infty$) is considered while, in practice, a stripline has a finite width. As a result, there is a slight deviation from the impedance characteristic foreseen by (4) and the actual, that is, from simulations, characteristic impedance. To compensate this, a desired characteristic impedance equal to $Z_d = 49\ \Omega$ is enforced. In this way, an actual characteristic impedance of 50 Ω is achieved.

Unfortunately, despite its simplicity, (4) contains elliptic integrals and hyperbolic functions (see [20] for details) and then (2) cannot be worked out to get $w_c(z)$ explicitly. Although an analytic solution in power series could be sought for, problem (2) is more easily solved numerically with a zero-finding algorithm. Particularly, problem (2) is solved over 101 evenly spaced points in the interval 0 mm $\leq z \leq l_1$. The z-distance between successive points is then $l_1/100 = 6.219$ mm. These points are joined with straight lines, creating the profile shown in Fig. 5. In the same figure also, the old linear design for $w_s(z)$ and the difference between old and new profiles are depicted. Note that the maximum difference between the profiles is less than 3 mm and that the new profile tends to become linear increasing the longitudinal coordinate. The derivative of the new profile $w_s(z)$ with respect to the longitudinal coordinate is greater closer to the feed and tends to become constant far away from it. The widths of new and old profiles are 20.7 and 26.0 mm at $z = 0$ mm, respectively.

The derived septum profile is fabricated of aluminum using a laser cutting machine achieving manufacturing tolerances in the 0.1-mm range. The new septum mounted on the TEM cell around a feed is depicted in Fig. 6 while the entire TEM cell with the new septum is shown in Fig. 1.

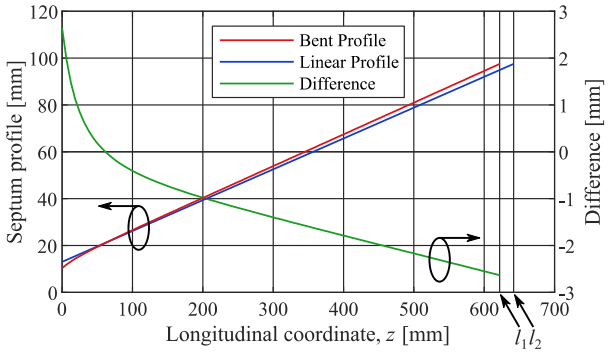

Fig. 5. Bent and linear profiles, and the difference between them. The coordinates refer to the septum top view of Fig. 4. The circles and the arrows upon them indicate the vertical scale to which the curves refer.

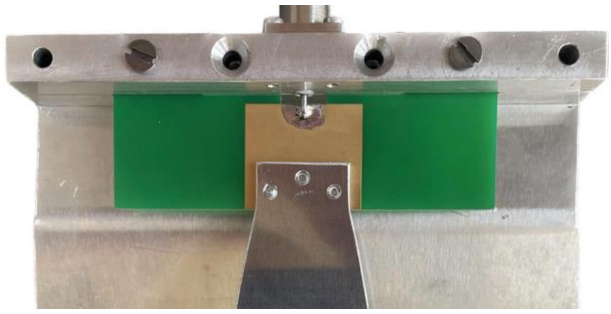

Fig. 6. Extremity of the new septum mounted on the TEM cell.

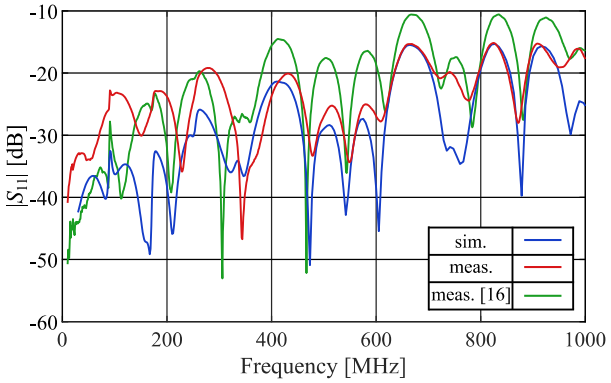

Fig. 7. Simulated and measured magnitudes of the scattering parameters.

The TEM cell is simulated in ANSYS HFSS [21] in the frequency interval 30 MHz–1 GHz considering the finite element method (FEM) solver and the broadband adaptive mesh. This frequency range is chosen to cover *CISPR* bands C and D. The TEM cell is measured in an anechoic chamber to avoid any influence of the surroundings.

Measured and simulated magnitudes of the S_{11} scattering parameter are depicted in Fig. 7. Measured data for the linearly tapered septum in [16] are also drawn. We notice an overall good agreement between simulations and measurements. Resonance frequencies from both measurements and simulations coincide well, even if minima in the magnitude of the reflection coefficient from measurements are generally less sharp. Furthermore, the deviations in the $|S_{11}|$, especially those for frequencies below 300 MHz, result from constructional and mounting imperfections and a limited vector network analyzer (VNA) accuracy for small magnitude values. The minimum value for the measured RL in the frequency range 30 MHz–1 GHz is 15.2 dB at 825 MHz. This value is 4.6 dB greater than the minimum value of RL for the TEM cell in [16] in the same bandwidth, thus proving the effectiveness of the proposed design method.

IV. Conclusion

A simple semianalytical design method based on dominant TEM-mode propagation for RL improvement in open TEM cells is presented. This method realizes a constant characteristic impedance along the tapering of the TEM cell, equal to the value of the characteristic impedance of both the feeds and the central stripline. The profile of the septum manufactured following the proposed approach differs less than 3 mm from the linear profile previously mounted on the same TEM cell. However, it improves remarkably the RL of 4.6 dB from 10.6 to 15.2 dB compared to the linearly tapered septum. The new minimum value of the RL is greater than the target value of 14 dB. In addition, the present method saves computational resources since it does not rely on optimizations.

As future developments, it would be interesting to perform a time-domain reflectometry analysis aimed at investigating the locations at which reflections occur and to develop advanced modeling techniques that help improve the TEM cell RL further.

Conflict of Interest

The authors have no conflict of interest to disclose.

References

[1] M. Mertens, M. Chavoshi, O. Peytral-Rieu, K. Grenier, and D. Schreurs, "Dielectric spectroscopy: Revealing the true colors of biological matter," *IEEE Microw. Mag.*, vol. 24, no. 4, pp. 49–62, Apr. 2023.

[2] G. Giannetti and K. Klinkenbusch, "Interpretation and separability of the effective permittivity in case that both permittivity and conductivity are complex," presented at the Electromagnetic Theory Symposium, Vancouver, BC, Canada, 2023.

[3] S. Yee, A. Sayegh, A. Kazemipour, and M. M. Jenu, "Design and calibration of a wideband TEM-cell for material characterization," in *Proc. Asia–Pacific Symp. Electromagn. Compat.*, 2012, pp. 749–752.

[4] M. Soueid et al., "Electromagnetic analysis of an aperture modified TEM cell including an ITO layer for real-time observation of biological cells exposed to microwaves," *Progr. Electromagn. Res.*, vol. 149, pp. 193–204, Nov. 2014.

[5] R. Videnka and J. Svacina, "Introduction to EMC pre-compliance testing," in *Proc. 17th Int. Conf. Microw. Radar Wireless Commun.*, 2008, pp. 1–4.

[6] S. M. Satav and V. Agarwal, "Do-it-yourself fabrication of an open TEM cell for EMC pre-compliance," in *Proc. IEEE EMC Soc. Newslett.*, 2008, pp. 66–71.

[7] P. F. Wilson and M. T. Ma, "Simple approximate expressions for higher order mode cutoff and resonant frequencies in TEM cells," *IEEE Trans. Electromagn. Compat.*, vol. EMC-28, no. 3, pp. 125–130, Aug. 1986.

[8] S. Deng, D. Pommerenke, T. Hubing, and D. Shin, "An experimental investigation of higher order mode suppression in TEM cells," *IEEE Trans. Electromagn. Compat.*, vol. 50, no. 2, pp. 416–419, May 2008.

[9] *CISPR 16-1-1 Specification for Radio Disturbance and Immunity Measuring Apparatus and Methods—Part 1-1: Radio Disturbance and Immunity Measuring Apparatus—Measuring Apparatus*, IEC Standard CISPR 16-1-1:2019, 2019.

[10] P. Alotto, D. Desideri, and A. Maschio, "Parametric analysis and optimization of the shape of the transitions of a two-port rectangular TEM cell," in *Proc. IEEE Int. Symp. Electromagn. Compat.*, 2012, pp. 1–6.

[11] K. Patel and P. Negi, "Importance and estimation of mismatch uncertainty for RF parameters in calibration laboratories," *Int. J. Metrol. Qual. Eng.*, vol. 3, no. 1, pp. 29–37, 2012.
[12] M. Arezoomand, M. K. Meybodi, and N. Noori, "Design of a TEM cell using both multi-step and piecewise linear tapering," in *Proc. 8th Int. Symp. Telecommun.*, 2016, pp. 571–574.
[13] M. L. Crawford, "Generation of standard EM fields using TEM transmission cells," *IEEE Trans. Electromagn. Compat.*, vol. EMC-16, no. 4, pp. 189–195, Nov. 1974.
[14] G. G. Gentili, G. Giannetti, G. Pelosi, and S. Selleri, "Transformation optics combined with line-integrals for fast and efficient mode matching analysis of waveguide devices," *IEEE J. Microw.*, vol. 3, no. 3, pp. 1051–1060, Jul. 2023.
[15] U. Balaji and R. Vahldieck, "Analysis of higher order modes in TEM cells and RCL using the mode matching method," in *Proc. Int. Conf. Electromagn. Interference Compat.*, 1995, pp. 259–262.
[16] C. Spindelberger, G. Giannetti, and H. Arthaber, "Increasing the test-volume of open TEM cells by using an asymmetric design," in *Proc. Kleinheubach Conf.*, 2022, pp. 1–4.
[17] R. P. Hecken, "A near-optimum matching section without discontinuities," *IEEE Trans. Microw. Theory Techn.*, vol. 20, no. 11, pp. 734–739, Nov. 1972.
[18] E. Costamagna and A. Fanni, "Asymmetric TEM cell impedance calculation," in *Proc. Inst. Elect. Eng. H-Microw. Antennas Propag.*, vol. 137, no. 5, pp. 318–320, 1990.
[19] M. Lucido, G. Panariello, and F. Schettino, "Accurate and efficient analysis of stripline structures," *Microw. Opt. Technol. Lett.*, vol. 43, no. 1, pp. 14–21, 2004.
[20] P. Robrish, "An analytic algorithm for unbalanced stripline impedance," *IEEE Trans. Microw. Theory Techn.*, vol. 38, no. 8, pp. 1011–1016, Aug. 1990.
[21] "Ansys—Engineering simulation software." ANSYS. 2022. [Online]. Available: https://www.ansys.com/

Open Access funding provided by 'Università degli Studi di Firenze' within the CRUI CARE Agreement